PRP Pharmacology Research & Perspectives
Open Access

ORIGINAL ARTICLE

Analysis of differential secondary effects of novel rexinoids: select rexinoid X receptor ligands demonstrate differentiated side effect profiles

Pamela A. Marshall[1], Peter W. Jurutka[1], Carl E. Wagner[1], Arjan van der Vaart[2], Ichiro Kaneko[1], Pedro I. Chavez[3], Ning Ma[2], Jaskaran S. Bhogal[1], Pritika Shahani[1], Johnathon C. Swierski[1] & Mairi MacNeill[1]

[1]School of Mathematical and Natural Sciences, New College of Interdisciplinary Arts and Sciences, Arizona State University, 4701 W Thunderbird Rd, Glendale, Arizona 85306
[2]Department of Chemistry, University of South Florida, 4202 E Fowler Ave CHE 205, Tampa, Florida 33620
[3]Biomedical Sciences Program, Midwestern University, 19555 N 59th Ave., Glendale, Arizona 86308

Keywords
Bexarotene, lipids, rexinoids, RXR, thyroid

Correspondence
Pamela A. Marshall, School of Mathematical and Natural Sciences, New College of Interdisciplinary Arts and Sciences, Arizona State University at the West Campus, MC 2352, P.O. Box 37100, Phoenix, AZ 85069.
Tel: 602-543-6143;
Fax: 602-543-6073;
E-mail: pamela.marshall@asu.edu

Funding Information
This work was supported by the National Institutes of Health National Cancer Institute [Grant 1 R15 CA139364-01A2] and the Della L. Thome Memorial Foundation.

Received: 7 August 2014; Revised: 28 November 2014; Accepted: 15 December 2014

Pharma Res Per, 3(2), 2015, e00122, doi: 10.1002/prp2.122

doi: 10.1002/prp2.122

Abstract

In order to determine the feasibility of utilizing novel rexinoids for chemotherapeutics and as potential treatments for neurological conditions, we undertook an assessment of the side effect profile of select rexinoid X receptor (RXR) analogs that we reported previously. We assessed pharmacokinetic profiles, lipid and thyroid-stimulating hormone (TSH) levels in rats, and cell culture activity of rexinoids in sterol regulatory element-binding protein (SREBP) induction and thyroid hormone inhibition assays. We also performed RNA sequencing of the brain tissues of rats that had been dosed with the compounds. We show here for the first time that potent rexinoid activity can be uncoupled from drastic lipid changes and thyroid axis variations, and we propose that rexinoids can be developed with improved side effect profiles than the parent compound, bexarotene (**1**).

Abbreviation

a-beta, amyloid beta; AD, activation domain; AD, Alzheimer's disease; AUC, area under the curve; GFP, green fluorescent protein; HDL, high-density lipoprotein; HRE, hormone-responsive element; LBD, ligand-binding domain; LBP, ligand-binding pocket; LDL, low-density lipoprotein; LXR, liver X receptor; PD, Parkinson's disease; PPAR, peroxisome proliferator-activated receptor; RAR, retinoic acid receptor; RXRE, RXR-responsive element; RXR, retinoid X receptor; SNuRMS, specific nuclear receptor modulators; SREBP, sterol regulatory element-binding protein; T3, thyroid hormone; TRE, thyroid hormone-responsive element; TR, thyroid hormone receptor; TSH, thyroid-stimulating hormone; VDR, vitamin D receptor.

Introduction

The retinoid X receptors (RXRs) comprise three isoforms in humans (α, β, and γ) (Leid et al. 1992; Mangelsdorf et al. 1994) all of which act as sequence-specific DNA-binding factors (transcription factors), often partnering with other transcriptional regulators in a larger superfamily of nuclear receptors including the liver X receptor (LXR), the thyroid hormone receptor (TR), the retinoic acid receptor (RAR), the vitamin D receptor (VDR), and the peroxisome proliferator-activated receptor (PPAR), to name a few. All of the above named nuclear receptors promote or regulate gene transcription when associated with the proper receptor ligand. This ligand, often consisting of an endogenous molecule, associates with the receptor ligand-binding domain (LBD) and this binding effects a conformational change that induces the receptor to interact with a corresponding hormone-responsive element (HRE) in DNA. While many HREs are located inside or proximal to the regulated gene's promoter

region, some HREs have been found considerably distant either downstream or upstream from their controlled genes. Typically, HREs comprise two minimal core hexad sequences such as AGGTCA and variants, with the orientation and spacing between which determining the binding mode (homodimer, heterodimer, or monomer) and identity of the nuclear receptor partner (Remenyi et al. 2004).

While VDR, TR, and RAR were first believed to bind as homodimers to their corresponding HREs (Forman et al. 1989), these nuclear receptors actually form heterodimers with RXR in order to bind to their HRE sites (Johnson et al. 1987; Mangelsdorf and Evans 1995). When bound with an agonist ligand, such as naturally occurring 9-*cis*-retinoic acid (9-*cis*-RA) or a synthetic agonist such as bexarotene (**1**), RXR forms a homodimer that subsequently associates with the RXR-responsive element (RXRE). When RXR acts as a partner in a heterodimer with another nuclear receptor, however, it may do so with or without a ligand bound to RXR depending on the heterodimer. For example, there is strong evidence that the LBP (ligand-binding pocket) of RXR is vacant in the functioning RXR-VDR heterodimer (Thompson et al. 2001). In the case of the RXR-LXR heterodimer, however, the LBP of RXR can be occupied (Svensson et al. 2003). Because of its ability to partner with numerous other nuclear receptors and subsequently associate with the heterodimer HRE, RXR has been described as the central nuclear receptor (Nahoum et al. 2007). Indeed, the observation that RXR possesses multiple dimerization surfaces to be able to pair with different nuclear receptors, yet it still retains the flexibility to associate with each heterodimeric HRE, contributes to the view of RXR as the master partner.

As observed earlier, there are two main classifications into which RXR-heterodimer complexes can be divided. These are commonly referred to as permissive or nonpermissive heterodimers, respectively. Permissive heterodimers can be actuated by either a ligand binding to RXR or a ligand binding to its partner, whereas a purely nonpermissive heterodimer can only function when a ligand binds to the primary (non-RXR) receptor (Forman et al. 1995). Nonpermissive heterodimers are generally exemplified by RXR-VDR, RXR-TR, and RXR-RAR. For the most part, but not always, RXR is "silent" in VDR and TR heterodimers, whereas RXR-RAR heterodimers are further activated by specific RXR ligands in addition to a RAR ligand. In fact, in a few cases, RXR ligands have been observed to promote RXR-RAR functioning, even when an RAR ligand is absent (Lala et al. 1996). Hence, the RXR-RAR heterodimer has been termed "conditionally" nonpermissive. In comparison to the nonpermissive heterodimers described earlier, the RXR-PPARs, RXR-FXRs, and RXR-LXRs are completely permissive heterodimers.

Developing therapeutic RXR-selective ligands is challenging not only because permissive RXR heterodimers may lead to off-target responses but also because in some tissue types, the availability of RXR may be limited. For example, the natural 9-*cis*-RA has been observed to inhibit the activation of the nonpermissive RXR-VDR (MacDonald et al. 1993; Lemon and Freedman 1996; Thompson et al. 1998) and RXR-TR heterodimers (Lehmann et al. 1993). The development of novel RXR-selective ligands (rexinoids) for therapeutic uses must thus be concerned with identifying compounds that exert RXR-heterodimer selectivity. Indeed, the approach of designing rexinoids that drive binding to specific nuclear receptor modulators (SNuRMs) is a topic of current interest.

As an FDA-approved drug, bexarotene (**1**) is also often used "off-label" to treat non-small cell lung cancer (Dragnev et al. 2007) and breast cancer (Esteva et al. 2003). While **1** and related RXR agonists have primarily been investigated as treatments for cancer, there have been recent reports of the exploration of **1** as a potential therapeutic for neurological conditions and diseases. For example, **1** was initially reported to clear amyloid plaques, lower levels of amyloid beta (a-beta) oligomers, and improve cognitive deficits in aggressive Alzheimer's disease (AD) mouse models (Cramer et al. 2012). However, some controversy surrounds the effectiveness of **1** in murine models of AD, since other groups replicating the original experiments did not observe similar reductions of a-beta or cognitive improvements though some groups did observe lowered levels of a-beta oligomers and cognitive improvements (Fitz et al. 2013; Price et al. 2013; Tesseur et al. 2013; Veeraraghavalu et al. 2013). One hypothesis suggests that **1** exerts a therapeutic effect in AD by upregulating ApoE (Holtzman 2004) and ABCA1 (Koldamova et al. 2005) expression via the activation of RXR:LXR and RXR:PPAR (Heneka et al. 2005), and this results in higher concentrations of larger HDL particles that prevent a-beta plaque formation (Fan et al. 2009). Indeed, on this basis alone, two clinical trials for **1** in AD patients are currently underway. Interestingly, a recent report by Fantini et al. (2014) suggests that **1** may be effective in preventing a-beta oligomers from forming calcium transport channels in neuronal cells by disrupting the oligomers' ability to bind to cholesterol, while another report (Tai et al. 2014) finds that **1** is more effective in later stage AD using a humanized ApoE mouse model.

In addition to AD, schizophrenia and Parkinson's disease (PD) are also neurological conditions for which **1** may exert a beneficial effect. In the case of schizophrenia, there is strong evidence of retinoid dysregulation (Goodman 1994) that could potentially be ameliorated by treatment with a potent retinoid such as **1**. Indeed, adding treatment with **1** to antipsychotic medications has been

shown to mitigate symptoms associated with schizophrenia (Lerner et al. 2008). In the case of PD, a recent report by Burstein and coworkers suggests that **1** interacts with the Nurr1-RXR heterodimer, at 100-fold lower doses than used in treatment of cancer, to restore dopamine neurons in rat models of PD (McFarland et al. 2013).

Although **1** is a potent RXR agonist, treatment for cancer at a dose up to 300 mg/m^2 per day nonetheless raises triglycerides–up to 2.5 times the upper limit of normal–as well as total cholesterol for most patients, and more than half of the patients experience hypothyroidism. While the raised triglyceride and cholesterol levels were observed to revert to normal levels following therapy cessation, the triglyceride and cholesterol levels were also observed to be clinically manageable with antilipidemic therapy during treatment with **1** (Eisai 2001).

Given the numerous applications of **1** in the treatment of several human cancers as well as its exploration as a potential therapy for several neurological diseases, we undertook the determination of pharmacokinetic parameters and side effect profiles of several novel analogs of **1** and other potent RXR agonists that we have recently synthesized. Our results show that the majority of our novel analogs–in cell-based assays or in Sprague–Dawley rats at 100 and 30 mg/kg–possess activities and side effect profiles not statistically different than **1**. However, in comparison with **1**, several of our novel compounds are potentially more bioavailable and thus could putatively be more useful therapeutically since a lower dose could be given than the standard dose (100 mg/kg) for **1**. Thus, our novel analogs represent theoretically viable therapeutics for several human cancers and possibly for the neurological diseases noted earlier, and we are continuing to explore their activities in these areas.

Materials and Methods

EC_{50} determination

Full dose−response curves, ranging from 1×10^{-9} to 0.3×10^{-5} mol/L ligand in transfected HCT-116 cells using an RXR mammalian two-hybrid system, were used to generate EC_{50} values. HCT-116 (male *Homo sapiens* colorectal carcinoma epithelium) cells were plated overnight at 80,000 cells/well in a 24-well plate and maintained as described previously (Wagner et al. 2009; Furmick et al. 2012; Jurutka et al. 2013). The cells were cotransfected using a human RXR binding domain (BD) vector, a human RXR activation domain (AD) vector, a luciferase reporter gene containing BD-binding sites, and Renilla control plasmid, using 2 μL/well of Express-IN transfection reagent (Thermo Fisher Scientific, Lafayette, CO) that was allowed to incubate for 24 h with the cells. The cells were then treated with ethanol vehicle (0.1%) or analogs (1.0, 2.5, 5.0, 7.5, 10, 25, 50, 75, 100, 250, 500 nmol/L, 1, 2, 3 μmol/L) and incubated for 24 h. The amount of rexinoid activity at each concentration was measured using the luciferase assay described earlier, and EC_{50} values were calculated using dose−response curves of ligand concentration versus normalized luciferase activity.

TR activation assay

The reporter construct (TRE-Luc [thyroid hormone-responsive element]) utilized for assaying TR signaling was constructed by inserting the double-stranded oligonucleotide, CTGGGAGGTGACAGGAGGACACGAGCTGG GAGGTGACAGGAGGACACGAG, with a *Bgl*II overhang on the 5′ end and a *Hind*III overhang on the 3′ end, upstream of a minimal promoter in the luciferase vector pLUC-MCS (Stratagene Corp., La Jolla, CA). This oligonucleotide contains two copies of the thyroid HRE (half sites are underlined) from the rat myosin heavy chain gene (Tsika et al. 1990). HCT-116 colorectal carcinoma cells were plated overnight at 80,000 cells/well in a 24-well plate and maintained in Dulbecco's modified Eagle's medium (DMEM)/High Glucose (Hyclone; GE Life Sciences, Logan, UT) enhanced with 10% fetal bovine serum (FBS) (Invitrogen, Life Technologies, Grand Island, NY), 1 mmol/L sodium pyruvate (Invitrogen, Life Technologies, Grand Island, NY), 100 μg/mL streptomycin (Invitrogen), and 100 U/mL penicillin (Invitrogen). The cells were cotransfected using 250 ng of TRE-Luc reporter gene, 50 ng of pSG5-hTR, and 20 ng of the Renilla control plasmid along with 2 μL/well of Express-IN transfection reagent (Thermo Fisher Scientific) used for liposome-mediated DNA delivery for 18 h. The cells were then incubated for 24 h post-transfection with ethanol vehicle or bexarotene or analogs (final concentration of 1×10^{-7} or 5×10^{-7} mol/L). After a 24-h incubation period, the amount of luciferase activity was measured using a luminescence assay. The amount of TRE activity was measured by luciferase output utilizing a dual-luciferase reporter assay system according to the manufacturer's protocol (Promega, Madison, WI) in a Sirius luminometer (Berthold Detection System, Pforzheim, Germany). Three independent assays were conducted with triplicate samples for each treatment group. Significance was analyzed by a two-tailed unpaired Student's *t*-test.

TR-TRE inhibition assay

The TR-TRE inhibition assay was completed using HCT-116 cells plated at 80,000 cells/well in a 24-well plate and maintained as described earlier. The cells were

cotransfected using 250 ng of the TRE-Luc reporter gene (described earlier), 50 ng of pSG5-hTR, and 20 ng of the Renilla control plasmid with 2 μL/well of Express-IN again used for liposome-mediated DNA delivery for 18 h. The cells were incubated for 24 h post-transfection with ethanol vehicle, 10^{-6} mol/L thyroid hormone (T3) alone, or 10^{-6} mol/L T3 in combination with bexarotene or analogs (final concentration of 1×10^{-7} or 5×10^{-7} mol/L). After a 24-h incubation period, the amount of luciferase activity was measured using the luminescence assay described earlier. Three independent assays were conducted with triplicate samples for each treatment group. Inhibition of T3 activity was determined by evaluation of T3-treated cells compared to cells treated with T3 plus bexarotene/analog. Significance was analyzed by a two-tailed unpaired Student's *t*-test.

Sterol regulatory element-binding protein activation assay

HCT-116 colorectal carcinoma cells were maintained as described earlier. The cells were cotransfected using 250 ng of the pBP1c(6500)-Luc reporter gene which contains an LXRE in the context of about 6500 base pairs of flanking DNA from the mouse sterol regulatory element-binding protein (SREBP)-1c natural promoter (Repa et al. 2000) along with 50 ng of CMX-hLXRα, 50 ng of pSG5-hRXRα, and 20 ng of the Renilla control plasmid. The transfection was initiated with 2 μL/well of Express-IN transfection reagent (Thermo Fisher Scientific) used for liposome-mediated DNA delivery for 18 h. The cells were then incubated for 24 h post-transfection with ethanol vehicle, 10^{-7} mol/L TO901317 alone, or 10^{-7} mol/L bexarotene/analogs alone, or the combination of the two ligands. After a 24-h incubation period, the amount of luciferase activity was measured using a luminescence assay. The amount of SREBP promoter activity was measured by luciferase output utilizing a dual-luciferase reporter assay system according to the manufacturer's protocol (Promega) in a Sirius luminometer (Berthold Detection System). Three independent assays were conducted with triplicate samples for each treatment group. Significance was analyzed by a two-tailed unpaired Student's *t*-test.

Cyprotex toxicity and mutagenicity analysis

This analysis was performed in-house at Cyprotex Labs (Watertown, MA). Each test compound is diluted into dimethyl sulfoxide (DMSO), subsequently diluted into water, and then added as a series of dilutions into a 96-well plate. Methyl methanesulfonate is added as a positive control for genotoxicity. The assay used two strains of cultured human lymphoblastoid TK6 cells, the test strain (GenM-T01) and the nonfluorescent control strain (GenM-C01), the latter was used to allow correction for any autofluorescence from the test compounds. The test strain has incorporated a patented green fluorescent protein (GFP) reporter system that exploits the proper regulation of the *GADD45a* gene, which mediates the adaptive response to genotoxic stress; exposure to a genotoxic compound increases expression of GFP.

Cells, media, and compound (1% DMSO final concentration; either alone or activated by a rat liver S9 extract) are added to a well to perform the assay. The microplates are covered with a breathable membrane and incubated at 37°C with 5% CO_2 and 95% humidity for 48 h. The plates are analyzed at 24 and 48 h time points using a microplate reader, reading both cell density and GFP expression. Fluorescence is normalized to the absorbance signal to correct for variation in cell yield caused by cytotoxicity. Raw data collected from GreenScreen assay plates are saved to an MS Excel file and analyzed by Cyprotex with GreenScreen Software, Cyprotex Labs, Watertown, MA.

Animal dosing

All in vivo work was performed by Covance Laboratories in Madison, WI. Covance has approval through the NIH OLAW (Office of Laboratory Animal Welfare); their assurance number is A3218-01. Approvals were obtained both from Covance IACUC and ASU IACUC before experiments commenced. All compounds were suspended in sesame oil, as in the original analysis at Ligand Pharmaceuticals (Howell et al. 2001) and as in other analyses (Tai et al. 2014), due to the hydrophobic nature of the compounds (Bolko et al. 2014) and to try to maximize drug absorption (Eisai 2001), at a final concentration of 10 mg/mL. Male Sprague–Dawley rats (8–12 weeks old and 250–350 g, obtained from Harlan Laboratories, Indianapolis, IN) were allowed to acclimate for over 2 days, fasted 24 h prior to a single dose at a target concentration 100 mg/kg for lipid analysis and PK analysis (Howell et al. 2001) and 30 mg/kg for thyroid-stimulating hormone (TSH) analysis (Liu et al. 2002), and then allowed to feed ad libitum 4 h post dose (Harlan Certified Rodent Diet #2016C or 2016CM and clean water). Dosing was done by oral administration using a blunt needle. Blood was drawn from three animals at the indicated time points, and processed for analysis. For lipid and pahrmacokinetic (PK) analysis, half of the sample was processed for plasma and half was allowed to clot and processed for serum. For TSH analysis, blood was drawn from animals at the indicated time points and allowed to clot and processed for serum.

Lipid analysis

Serum was analyzed for cholesterol, high-density lipoprotein (LDL), low-density lipoprotein, and triglycerides using a Lipid Profile Panel at Covance. For the LC-MS/MS analysis, the plasma samples are prepared by liquid–liquid extraction using ethyl acetate. Following extraction, the supernatant is transferred to a new plate and evaporated under nitrogen. The samples are then reconstituted using mobile phase B for injection on the instrument. The LC-MS/MS instrument comprised a Shimadzu HPLC (Columbia, MD) and a API5000 mass spectrometer. Chromatographic separation is achieved using a C18 column in conjunction with gradient conditions (ammonium acetate/acetic acid in water [A] or 80:20 ACN:water [B]). MS detection is accomplished through monitoring of MRM transitions unique to each analyte in negative mode. The calibration curves range from 1 to 20 (depending on the analyte) to 1000 ng/mL, and no QC samples are included. The clinical pathology samples are analyzed using a Roche Modular P instrument (InIdianapolis, IN).

TSH analysis

Serum was analyzed via enzyme-linked immunosorbent assay (ELISA) (Catalog No. KT-29925; Kamiya Biomedical Company, Seattle, WA) for TSH concentration analysis according to manufacturer's instructions. An unpaired heteroscedastic two-tailed Student's *t*-test was employed to determine if the decrease in the TSH in each case was statistically different than the bexarotene treatment.

PK analysis

Plasma was analyzed via liquid chromatography and tandem mass spectrometry for compound concentration. Whenever possible, determination of maximum concentration (C_{max}), time to maximum concentration (T_{max}), and total area under the curve (AUC) was performed. Pharmacokinetic parameters are calculated by noncompartmental analysis using WinNonlin Professional Edition (Version 5.2; Pharsight Corporation, Princeton, NJ). Nominal doses and sampling time points were used for all groups.

UV-vis ε and water solubility determinations

A 2.0 mmol/L stock solution in ethanol of **1**, **2**, **4**, **7**, **9**, and **14** was made from which ε was determined from a Beer's law plot of dilutions. A 10 μmol/L solution in 10% ethanol/water of **1** and each compound was also made by dissolving 0.020 mmol of **1**, **2**, **4**, **7**, **9**, and **14** in 200 mL of ethanol and then diluting to 2.0 L with water. Dilutions of the 10 μmol/L solution in 10% ethanol/water were made to determine an equation for the Beer's law plot by linear regression. Saturated aqueous solutions at 20°C of **1**, **2**, **4**, **7**, **9**, and **14** were prepared by placing ~25 mg of micronized compound in 10 mL of deionized water and agitating, intermittently, for 24 h, and filtering with a 0.22 μm Millipore filter (Darmstadt, Germany). The water solubility of **1**, **2**, **4**, **7**, **9**, and **14** was estimated by solving the linear regression equation from the Beer's law plot for the 10% ethanol/water solutions with the observed absorbance of the saturated aqueous solutions of **1**, **2**, **4**, **7**, **9**, and **14**.

pK_a calculations

Absolute pK_as were calculated using the thermodynamic cycle shown in Figure 1 (Shields and Seybold 2013). All protonated and deprotonated structures were geometry optimized at the B3LYP/6-311+G(d,p) level, and the nature of the minimum was confirmed by harmonic frequency calculations. The scaled frequencies (Merrick et al. 2007) were then used to calculate gas-phase free energies. The solvation free energies ΔG_s of the optimized structures were calculated using the SM8 continuum model (Marenich et al. 2009) at the B3LYP/6-311+G(d,p) level. For the proton, experimentally derived values of −6.28 kcal/mol for the gas-phase free energy and −264.61 kcal/mol for the solvation free energy were used. All calculations were performed with Gaussian 09 (Frisch et al. 2009).

RNA sequencing analysis

Brains from animals treated above were removed and snap frozen in liquid nitrogen and then sent to LabCorp Clinical Trials (formerly Covance Genomics Lab) where they were suspended in 500 μL of RLT buffer (Qiagen, Valencia, CA) containing β-mercaptoethanol and homogenized using a Covaris homogenizer (Woburn, MA). Following trizol/chloroform treatment, RNA was extracted

$$\begin{array}{ccccc} AH_{gas} & \xrightarrow{\Delta G_{gas}} & A^-_{gas} & + & H^+_{gas} \\ \uparrow -\Delta G_s(AH) & & \downarrow \Delta G_s(A^-) & & \downarrow \Delta G_s(H^+) \\ AH_{aq} & \xrightarrow{\Delta G_{aq}} & A^-_{aq} & + & H^+_{aq} \end{array}$$

Figure 1. Thermodynamic cycle used in calculating pK_a.

using Promega SV96 isolation kits. RNA was qualified using an Agilent Bioanalyzer and quantified using ribogreen. RNA_Seq libraries were constructed using Illumina's TruSeq™ Total RNA strand specific kits (San Diego, CA) with 250 ng of total RNA. Briefly, rRNA was removed from FF or FFPE total RNA using Epicentre's Ribo-Zero GOLD rRNA Removal kit (Madison, WI). Ribo-Zero RNA was then incubated with Random Primers (Invitrogen, Grand Island, NY) at 65°C for 5 min. Illumina TruSeq™ RNA Sample Prep Kit was then used to construct the library according to the manufacturer's protocol from the step of first strand cDNA synthesis. The sequencing libraries were quality controlled using an Agilent 2100 Bioanalyzer and quantified using qPCR prior to cluster generation on an Illumina cBot. Sequence data were generated on Illumina HiSeq instruments as paired end 51-bp reads, following the manufacturer's protocols using TruSeq SBS v3 chemistry. An in-house pipeline for analysis, which integrates several open source programs, was used to analyze data. Briefly, initial FASTQ files were subjected to quality control with the FastQC tool. Raw reads from each capture library were aligned to the rat reference genome (rn5) with STAR version 2.3.1r, using default parameters. Expressed transcriptome was built using Cufflinks (version 2.1.1) and was annotated using cuffmerge (Cufflinks version 2.1.1). The rn5 refGene.gtf annotation (UCSC), filtered to include only canonical chromosomes was used as the reference GTF.

Results

Rexinoid structures and EC_{50} values

Figure 2 depicts the structures of the compounds we utilized for the assays. Bexarotene (**1**) is the standard by which the rexinoids were compared, as it is the FDA-approved drug. Characteristics of these compounds and their synthesis were described in our previous work (Wagner et al. 2009; Furmick et al. 2012; Jurutka et al. 2013). In Table 1, we summarize the EC_{50} values for these compounds.

TRE activation via select rexinoids

In order to assess potential side effect differences between our rexinoids, we first utilized a cell culture model. We assessed the ability of each rexinoid to bind to RXR and allow the receptor to act as a permissive partner to acti-

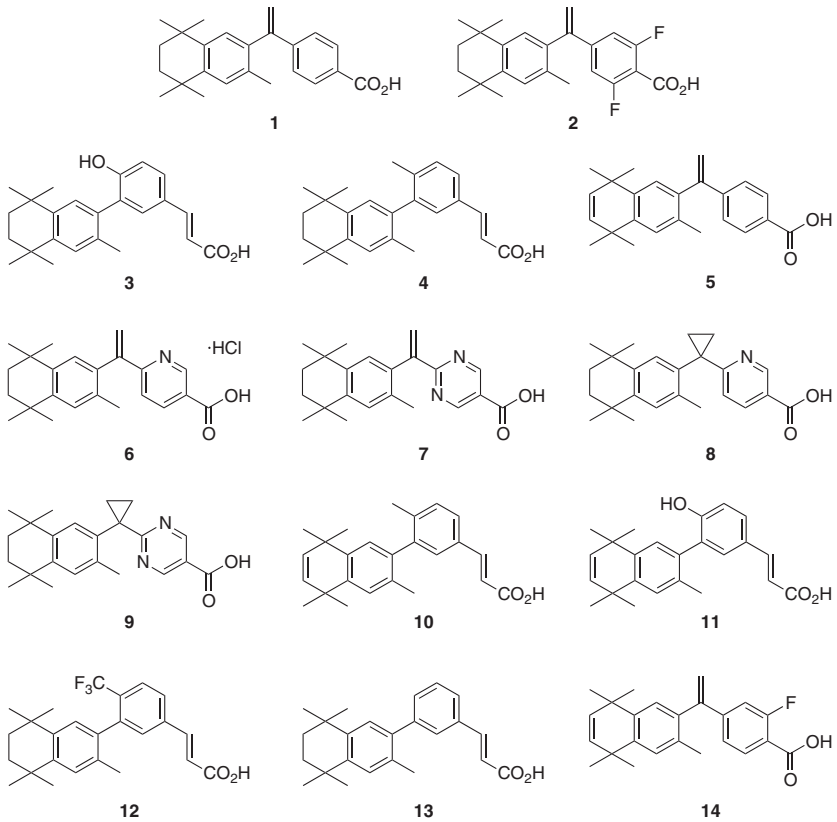

Figure 2. Structures of rexinoids analyzed in this article.

Table 1. EC_{50} values of compounds evaluated in this study.

Compound	EC_{50} value[1] nmol/L (±SD)
Compound **1**	55 (6)
Analog **2**	34 (6)
Analog **3**	13 (3)
Analog **4**	42 (3)
Analog **5**	74 (7)
Analog **6**	21 (2)
Analog **7**	44 (12)
Analog **8**	15 (3)
Analog **9**	50 (10)
Analog **10**	72 (11)
Analog **11**	15 (2)
Analog **12**	69 (7)
Analog **13**	109 (8)
Analog **14**	71 (10)

RXR, rexinoid X receptor.

[1]EC_{50} values were determined from full dose–response experiments with each compound in the range of 10^{-9} to 10^{-5} mol/L in transfected HCT-116 cells using an RXR mammalian two-hybrid system.

vate an RXR/TR heterodimer in the absence of thyroid hormone (Castillo et al. 2004) at two concentrations (1×10^{-7} and 5×10^{-7} mol/L). The cells were transfected with TR and a TRE (thyroid hormone-responsive element) driving a luciferase reporter gene, so that RXR was in limiting concentrations. As can be seen in Figure 3, each rexinoid (except analog **8**) can significantly ($P < 0.05$) stimulate RXR to act as a permissive partner (in the absence of thyroid hormone) with the TR at 1×10^{-7} mol/L of analog (Fig. 3A), but not at 5×10^{-7} mol/L (Fig. 3B). Since RXR is limiting, at a higher concentration of ligand (5×10^{-7} mol/L) the rexinoids may be driving formation of RXR homodimers rather than acting to stimulate RXR/TR heterodimers, and/or some of the analogs result in a TR-RXR heterodimer conformation that recruits corepressors to the transcriptional complex resulting in either no activation or even repression below ethanol vehicle levels (Fig. 3B, analogs **8**, **11**–**14**).

Rexinoid inhibition of T3-stimulated TR-TRE transcription

Hypothyroidism is a widely reported problem with bexarotene treatment (Sherman et al. 1999), and is thought to occur partly because bexarotene stimulates RXR homodimers, which in turn diverts the RXR away from partnering with TR. We utilized a TRE-linked reporter vector and cell culture system in which cells were treated with both a thyroid hormone (T3) and a rexinoid to determine the percentage of inhibition by the rexinoid treatment. In this system, RXR is limiting and thus adding a rexinoid should stimulate RXR homodimerization, and remove the RXR from the RXR/TR heterodimer, blunting the T3 response, as assayed by TRE activation. As shown in Figure 4, each rexinoid demonstrates a different inhibition profile, with analogs **3** and **8** demonstrating the most inhibition at 1×10^{-7} mol/L (Fig. 4A, $P < 0.01$) and at 5×10^{-7} mol/L (Fig. 4B) analogs **3**, **4**, **6**, **7**, **8**, **12**, **13**, and **14** inhibit the TRE-mediated activation significantly ($P < 0.01$).

More important than the inhibition profile, is the series of analogs that show little inhibition in this assay. This lack of inhibition hints that rexinoids, even with excellent RXRE activation profiles (Wagner et al. 2009; Furmick et al. 2012; Jurutka et al. 2013), and EC_{50}s comparable to bexarotene (Table 1) can be synthesized that, with the correct chemistry and binding profile, may alleviate or minimize thyroid hormone axis side effects. At a concentration of 1×10^{-7} mol/L, compounds **2**, **5**, **6**, **7**, **10**, **11**, **12**, **13**, and **14** demonstrate at least 85% (or more) of the activity of T3 alone (second bar from left), with less inhibition than **1** (bexarotene), and indeed **2**, **5**, **6**, **7**, **10**, **12**, and **13** are statistically the same as T3 alone (using a two-tailed heteroscedastic *t*-test). While at treatment concentration of 5×10^{-7} mol/L, we observe that compounds **9** and **10** show no inhibition of the T3 stimulation. Our novel results indicate that it is possible to uncouple the thyroid inhibition from the RXRE activation of rexinoid compounds and suggests a potential method to alleviate one of the untoward side effects of rexinoid treatment.

Activation of SREBP promoter-induced transcription of rexinoids

In order to assess potential lipid profile side effects, analysis of transcription driven by the SREBP promoter was undertaken. SREBP is a transcription factor that drives expression of genes involved in lipid synthesis by binding to a sterol regulatory element in DNA and promoting transcription. SREBP expression is driven in part by RXR/LXR binding to the SREBP promoter and stimulating transcription. To determine the ability of each rexinoid to stimulate SREBP expression, as a proxy for analysis of lipid anomalies induced by rexinoid treatment, we analyzed luciferase expression driven by the SREBP promoter in cells treated with rexinoid alone or in combination with T0901317 (T0), an LXR selective ligand. Each rexinoid was analyzed for its ability to stimulate transcription (Fig. 5) with and without T0, and we observed a range of activities. With analog alone, compounds **2**, **3**, **4**, **9**, **10**, and **13** demonstrated a similar transcriptional profile to bexarotene; while the remainder of the compounds showed an increased transcriptional response ($P < 0.05$, using a two-tailed heteroscedastic *t*-test). In

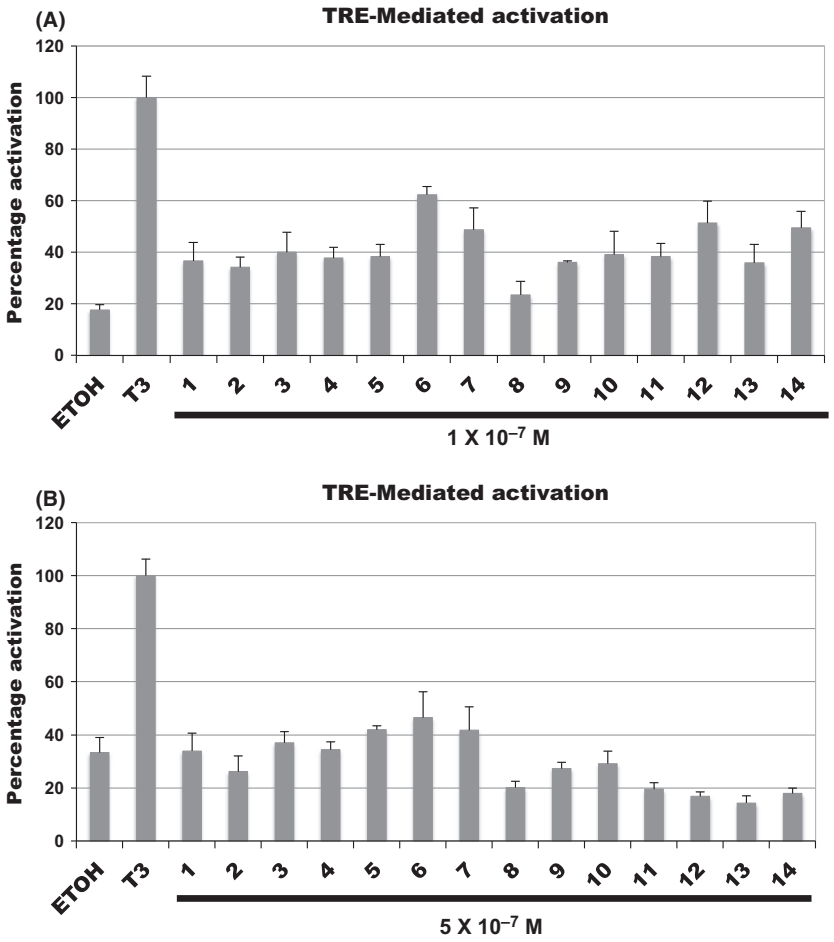

Figure 3. Thyroid hormone-responsive element (TRE) activation of select analogs. HCT-116 cells were transfected with thyroid receptor and a TRE driving luciferase, and luciferase activity was plotted as percentage of T3 response, which was normalized to 100%. Cells were treated with 1×10^{-6} mol/L T3 and 1–4 at (A) 1×10^{-7} mol/L and (B) 5×10^{-7} mol/L for 24 h.

analyzing rexinoids with T0, we saw a similar pattern, with compounds **2**, **4**, **7**, **10**, **12**, and **13** possessing similar activation to bexarotene (**1**) + T0 treatment. In contrast, with analog plus T0 treatment, only compounds **3** and **9** demonstrated *lower* SREBP promoter activation ($P < 0.05$). Interestingly, compounds **5**, **6**, **8**, **11**, and **14** showed higher activation ($P < 0.05$, using a two-tailed heteroscedastic *t*-test).

Select rexinoids show similar cytotoxicity profiles to bexarotene

Considering multiple characteristics, such as transcriptional activation of RXR based on reported EC_{50} values (Table 1) and performance in SREBP promoter activation assays (Fig. 5), we selected compounds **2**, **4**, **7**, **9**, and **14** as compounds to further explore as potential leads. To assess cytotoxicity and mutagenicity of these compounds prior to any in vivo studies, a GreenScreen™ assay was performed by Cyprotex. Compounds are solubilized in DMSO and added at several concentrations to a genetically modified human lymphoblastoid TK6 cell line, carrying the GFP gene driven by the *GADD45a* promoter. Compounds were either added alone or after activation with an S9 rat liver extract. Cytotoxicity was measured by a cell viability assay and genotoxicity (mutagenicity) was assayed by GFP fluorescence normalized to cell count. As seen in Table 2, bexarotene (**1**) is cytotoxic at 1.12 μg/mL without S9 activation and at 18 μg/mL with S9 activation, and is not genotoxic. These novel rexinoids show similar ranges of cytotoxicity as bexarotene, and only **14** demonstrates genotoxicity, at the same concentration that it is demonstrated to be cytotoxic; thus, this genotoxicity would never be clinically relevant as the dose is too high to be useful because that dose is also cytotoxic as well. Notably, **9**, an analog of LGD100268, was the least

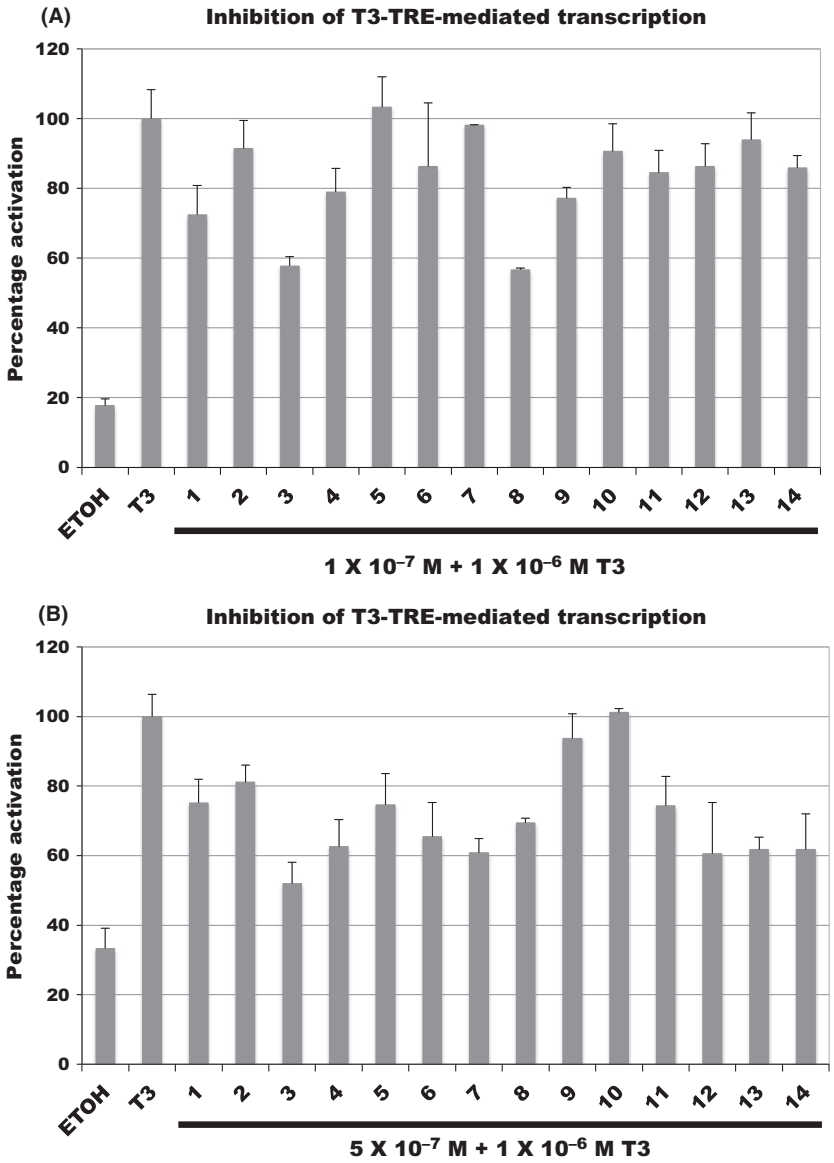

Figure 4. Select rexinoids inhibit thyroid hormone-responsive element (TRE) activation by T3. HCT-116 cells were transfected with thyroid receptor and a TRE driving luciferase, and luciferase activity was plotted as percentage of T3 response, which was normalized to 100%. Cells were treated with 1×10^{-6} mol/L T3 or with **1**–**14** at (A) 1×10^{-7} and 10^{-6} mol/L T3 and (B) 5×10^{-7} and 10^{-6} mol/L T3, for 24 h.

cytotoxic without S9 activation (up to 8.57 μg/mL), and **9** was the only analog that showed no cytotoxicity or genotoxicity with S9 activation. Thus, these new rexinoids have potential as therapeutics as they demonstrate similar toxicity patterns to bexarotene.

Select rexinoids have the same primary TSH phenotype as bexarotene

Bexarotene treatment often induces hypothyroidism in patients (e.g., Sánchez-Juan et al. 2007). In order to assess the side effect profiles of our novel rexinoids, male Sprague–Dawley rats were dosed at 30 mg/kg and TSH was assayed over a 24 h time course. The suppression of TSH occurs acutely due to the inhibition of the secretion of TSH from the pituitary (Liu et al. 2002), but after 16 h (or less) this inhibition is due to repression of the TSH promoter itself (Sherman et al. 1999). As seen in Figure 6, TSH decreased in all animals treated with rexinoid in the same manner with the same time course as bexarotene (**1**), with no statistically significant differences, indicating that these RXR ligands have no worse side effect profile over the first 24 h of treatment than the parent compound, bexarotene.

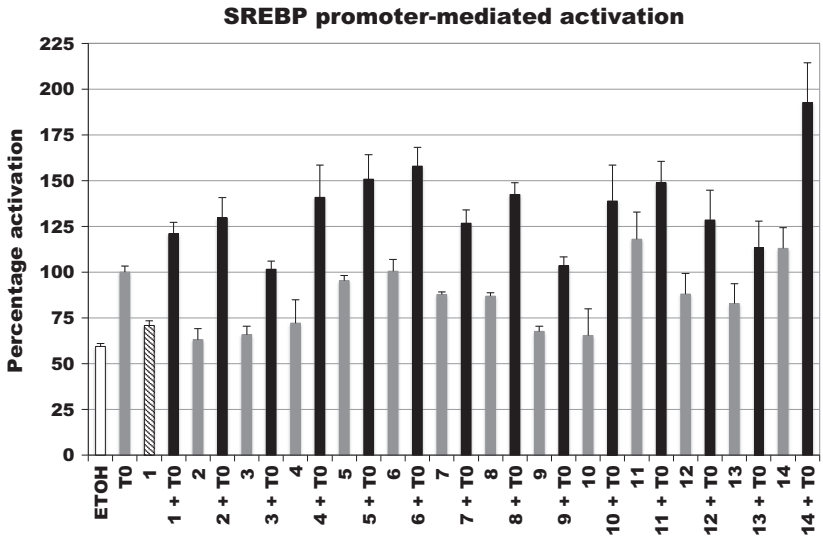

Figure 5. Select rexinoids potentiate SREBP promoter activation in the presence of T0901317. HCT-116 cells were transfected with LXRα, RXRα, and the SREBP promoter driving luciferase, and luciferase activity was plotted as percentage of T0901317 response (crosshatched bar), which was normalized to 100%. Cells were treated with 1×10^{-7} mol/L analog with or without 1×10^{-7} mol/L T0901317 for 24 h. LXR, liver X receptor; RXR, rexinoid X receptor; SREBP, sterol regulatory element-binding protein.

Select rexinoids show distinct lipid profiles from bexarotene (1)

Bexarotene (**1**) treatment increases plasma triglycerides and cholesterol in patients (e.g., Sánchez-Juan et al. 2007). To evaluate our rexinoids for potential differences in side effects, we treated male Sprague–Dawley rats with a single dose of 100 mg/kg bexarotene or analog and assessed cholesterol, LDL, HDL, and triglycerides at several time points.

Treatment of rats with **1** mimics published studies in mice, and several analogs have similar side effect profiles. In rats treated with **1**, total cholesterol actually goes down over a 24 h period (Table 3). This is reminiscent of mice treated with **1**, where the drop in total cholesterol is postulated to be due to inhibition of absorption of dietary cholesterol (de Vries-van der Weij et al. 2009). Only analog **14** has statistically significantly different (higher) cholesterol than bexarotene at 9 and 24 h. Treating rats with rexinoids generally did not affect the HDL (Table 4), and decreases the LDL (Table 5), similar to studies performed in mice (de Vries-van der Weij et al. 2009).

Only the triglyceride profiles of rats treated with **1** or any of the analogs differed significantly over the time course (Table 6). Triglycerides increase in patients treated with **1** (Sánchez-Juan et al. 2007) and this clinically is the most troublesome side effect in the lipid metabolism pathway, due to the predisposition to atherosclerosis and cardiovascular disease (Talayero and Sacks 2011). After 24 h, analog **14** induced significantly higher triglycerides (1589 ± 820.9 ng/dL vs. 279 ± 67.1 ng/dL with **1** treated animals), and rats treated with analogs **4** (109 ± 16.4 ng/dL) and **9** (158 ± 46.5 ng/dL) had lower triglycerides than rats treated with bexarotene. Thus, we have developed a series of rexinoids that can modulate lipid chemistry differently, although these analogs all bind and activate RXR in a similar manner (Wagner et al. 2009; Furmick et al. 2012; Jurutka et al. 2013).

Table 2. GreenScreen™ (Cyprotex) analysis of rexinoids for cytotoxicity and mutagenicity.

	Without S9 activation		With S9 activation	
	Cytotoxicity (μg/mL)	Genotoxicity	Cytotoxicity (μg/mL)	Genotoxicity
1	1.12	None	18	None
2	0.74	None	47.3	None
4	1.33	None	21.3	None
7	6.64	None	213	None
9	8.57	None	None	None
14	1.06	None	33.9	33.9 μg/mL

Rexinoids were added to TK6 cells to assess cytotoxicity and mutagenicity, as assayed by cell viability (cytotoxicity) and GFP expression (mutagenicity). Shown is the lowest effective concentration (LEC) for a positive result.

Pharmacokinetic profiles of bexarotene and select rexinoids in rats

We were interested in determining the pharmacokinetic profiles of bexarotene and several analogs in order to

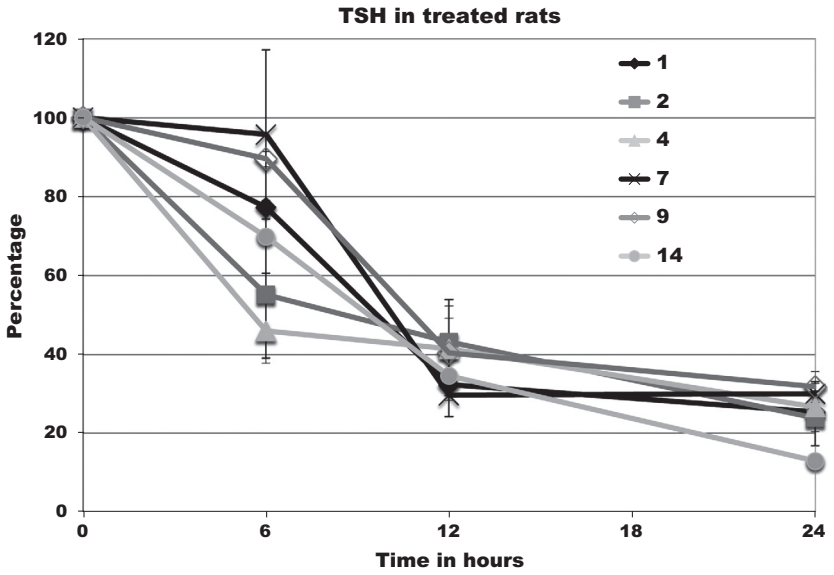

Figure 6. TSH levels in rats treated with rexinoids. TSH decreases in rats treated with bexarotene (**1**) or analogs. Male rats were treated with 30 mg/kg compound and blood was drawn predose, at 6, 12, and 24 h. TSH was quantitated by ELISA and represented as percentage of predose levels. TSH, thyroid-stimulating hormone.

Table 3. Blood cholesterol concentration after treatment of 100 mg/kg compound or vehicle control.

	Predose	1 h	2 h	3 h	6 h	9 h	12 h	24 h
Vehicle	110 ± 12.5	104 ± 12.1	94 ± 11.2	93 ± 8.4	101 ± 9	103 ± 13.4*	94 ± 8.7*	82 ± 2.1*
Bexarotene	105 ± 7.2	108 ± 14.4	93 ± 15.3	91 ± 9.6	89 ± 15.6	73 ± 10.7^	61 ± 13.8^	52 ± 6.6^
2	100 ± 21.2	122 ± 17.2	78 ± 6.2	95 ± 16.5	71 ± 12.8^	80 ± 14	65 ± 13^	47 ± 8^
4	106 ± 1	100 ± 16.1	87 ± 4.9	81 ± 14.8	83 ± 7.5^	66 ± 15.1^	66 ± 10.6^	50 ± 11^
7	108 ± 12	107 ± 20.1	92 ± 17.5	85 ± 12.9	89 ± 16	73 ± 10.7^	62 ± 4.7^	47 ± 7.5^
9	91 ± 8.1	99 ± 7.5	81 ± 6.5	80 ± 10.8	75 ± 4.7^	68 ± 9.9^	50 ± 4.5^	49 ± 5.7^
14	111 ± 13.7	124 ± 6.7	98 ± 9.0	102 ± 12.5	97 ± 10.4	93 ± 12.5*	72 ± 11.9^	100 ± 21*

Male Sprague–Dawley rats were treated with 100 mg/kg compound in sesame oil or sesame oil alone (vehicle control). Blood was taken at the indicated time points and analyzed for cholesterol composition in mg/dL. Statistical analysis was performed using a one-tailed Mann–Whitney test. Statistically significantly different than: *bexarotene treatment $P \leq 0.05$; ^vehicle control $P \leq 0.05$.

Table 4. Plasma high-density lipoprotein concentration after treatment of 100 mg/kg compound or vehicle control.

	Predose	1 h	2 h	3 h	6 h	9 h	12 h	24 h
Vehicle	86 ± 14	85 ± 12.6	73 ± 11.9	67 ± 10.8	55 ± 4.0	65 ± 7.5	55 ± 6.4*	68 ± 4.5*
Bexarotene	83 ± 2.9	82 ± 15.2	63 ± 8.0	57 ± 9.0	47 ± 7.0	55 ± 7.0	34 ± 3.2^	37 ± 7.6^
2	82 ± 16.4	109 ± 11.8*^	67 ± 3.5	84 ± 13.6*	52 ± 10.8	61 ± 3.8	46 ± 12.1	30 ± 4.4^
4	81 ± 2.0	79 ± 13.2	66 ± 6.1^	57 ± 10.0	50 ± 4.0	56 ± 11.6	39 ± 5.0^	43 ± 9.5^
7	81 ± 10.8	74 ± 4.0	65 ± 13.1	54 ± 6.4	52 ± 12.3	48 ± 20.0	30 ± 10.8^	37 ± 3.1^
9	71 ± 6.9*	81 ± 3.6	65 ± 7.0	59 ± 4.2	47 ± 6.0	51 ± 3.2^	33 ± 4.9^	41 ± 3.6^
14	89 ± 7.2	99 ± 7.0*^	80 ± 7.5*	76 ± 12.8	58 ± 11.0	59 ± 7.0	39 ± 3.2^	61 ± 23.4

Male Sprague–Dawley rats were treated with 100 mg/kg compound in sesame oil or sesame oil alone (vehicle control). Blood was taken at the indicated time points and analyzed for HDL composition in mg/dL. Statistical analysis was performed using a one-tailed Mann–Whitney test.
*indicates statistically significantly different than bexarotene treatment $P \leq 0.05$; ^indicates statistically significantly different than vehicle control $P \leq 0.05$.

Table 5. Plasma low-density lipoprotein concentration after treatment of 100 mg/kg compound or vehicle control.

	Predose	1 h	2 h	3 h	6 h	9 h	12 h	24 h
Vehicle	31 ± 6.1	25 ± 5.0	22 ± 4.0	22 ± 3.1	29 ± 3.8*	30 ± 9.5*	25 ± 6.4*	20 ± 1.5*
Bexarotene	30 ± 4.0	27 ± 8.0	19 ± 5.0	16 ± 3.8	6 ± 2.6^	7 ± 1.2^	5 ± 4.0^	3 ± 0^
2	26 ± 7.6	27 ± 6.1	14 ± 6.1^	13 ± 3.6^	7 ± 1.5^	6 ± 1.2^	7 ± 2.0^	3 ± 0^
4	28 ± 2.1	27 ± 8.0	15 ± 8.0^	14 ± 7.5	7 ± 3.5^	8 ± 3.0^	5 ± 1.5^	7 ± 0*^
7	33 ± 1.7	36 ± 11.1	19 ± 11.1	19 ± 8.1	13 ± 1.5*^	11 ± 7.0^	6 ± 2.5^	4 ± 1.0^
9	25 ± 4.2	27 ± 3.5	16 ± 3.5	15 ± 4.5	9 ± 5.5^	7 ± 2.1^	5 ± 1.5^	4 ± 1.2^
14	33 ± 5.3	35 ± 2.6^	19 ± 2.6	18 ± 2.5	9 ± 3.6^	5 ± 2.5^	4 ± 1.0^	3 ± 0^

Male Sprague–Dawley rats were treated with 100 mg/kg compound in sesame oil or sesame oil alone (vehicle control). Blood was taken at the indicated time points and analyzed for LDL composition in mg/dL. Statistical analysis was performed using a one-tailed Mann–Whitney test.
*indicates statistically significantly different than bexarotene treatment $P \leq 0.05$; ^indicates statistically significantly different than vehicle control $P \leq 0.05$.

Table 6. Blood triglyceride concentration after treatment of 100 mg/kg compound or vehicle control.

	Predose	1 h	2 h	3 h	6 h	9 h	12 h	24 h
Vehicle	41 ± 8.4	75 ± 11.8	84 ± 11	114 ± 33.3	144 ± 86.7*	123 ± 49.8	115 ± 47.1	48 ± 12.1*
Bexarotene	35 ± 13.1	85 ± 21.4	98 ± 18.5	157 ± 79	444 ± 220.7^	160 ± 65.4	233 ± 138.9	279 ± 67.1^
2	35 ± 8.0	50 ± 19.1	53 ± 14.5*^	123 ± 38.9	191 ± 56.7	221 ± 99.6	181 ± 12.2^	436 ± 226.8^
4	50 ± 8.1	68 ± 5.9	118 ± 21.6^	146 ± 36.9	357 ± 306.9	123 ± 27	269 ± 101.5^	109 ± 16.4*^
7	38 ± 7.2	71 ± 29.6	130 ± 50.8	164 ± 122.3	217 ± 60.1*	290 ± 313.3	352 ± 355.3*	193 ± 77.3^
9	40 ± 15.6	36 ± 6.4*^	82 ± 16.5	118 ± 8.9	229 ± 93.0	177 ± 121.0	136 ± 22.2*	158 ± 46.5*^
14	37 ± 6.4	33 ± 1.7 *^	98 ± 18.2	113 ± 7.8	268 ± 58	340 ± 181.7^	286 ± 73.7^	1589 ± 820.9*^

Male Sprague–Dawley rats were treated with 100 mg/kg compound in sesame oil or sesame oil alone (vehicle control). Blood was taken at the indicated time points and analyzed for triglyceride composition in mg/dL. Statistical analysis was performed using a one-tailed Mann–Whitney test.
*indicates statistically significantly different than bexarotene treatment $P \leq 0.05$; ^indicates statistically significantly different than vehicle control $P \leq 0.05$.

determine if any rexinoid would show promise for additional research. As can be seen in Table 7 and Figure 7, the PK profiles of the RXR ligands varied markedly. Although each rat received the same 100 mg/kg dose, C_{max} (peak plasma concentration) varied greatly, from a low of 4913 ng/mL in analog **4** to a high of 44,000 ng/mL for analog **7**. All of the analogs have short T_{max}, of between 1 and 2 h. Although, interestingly, AUC does not always correlate with C_{max}, as some of the compounds may have a very long half-life (Fig. 7). For example, although the peak plasma concentration of bexarotene (**1**) is 8,523 ng/mL, the AUC is 51,531 ng/mL, more similar to **9**. Compound **14** appears to be cleared least effectively (Fig. 7) and **4** is at the lowest concentration in the plasma after 24 h.

Table 7. Pharmacokinetic profiles of **1** and analogs **2**, **4**, **7**, **9**, and **14** in male Sprague–Dawley rats that were treated with 100 mg/kg compound in sesame oil.

Compound	C_{max} (ng/mL)	T_{max} (h)	AUC_{0-t} (h × ng/mL)	AUC_{0-inf} (h × ng/mL)
Bexarotene	8,523.33	2	51,531.67	54,329.87
2	2,406.67	1	20,539.37	ND
4	4,913.33	2	24,650.67	24,735.07
7	44,000.00	1	83,343.87	83,984.92
9	25,400.00	1	50,444.23	51,483.03
14	18,633.33	1	152,955.83	ND

Rats were treated with compound and blood samples were taken to determine pharmacokinetic profiles by liquid chromatography and tandem mass spectrometry. ND, not determined; AUC, area under the curve.

Solubility and calculated pK_a of rexinoids studied in rats

The compounds demonstrated such different C_{max} and AUC values, as well as PK profiles (Fig. 7), we hypothesized that these properties of the compounds were affected by the physiochemical properties of the compounds. To explore this possibility, we performed water solubility determinations and calculated the pK_a values for **1** and analogs **2**, **4**, **7**, **9**, and **14**.

Water solubilities, as well as UV-vis absorptivity constants in pure ethanol and 10% ethanol/water (v/v), for **1** and analogs **2**, **4**, **7**, **9**, and **14** were determined at 20°C and summarized in Table 8.

As might be expected, the difluoro-bexarotene analog (**2**) was more soluble (58 μmol/L) than **1** (0.28 μmol/L),

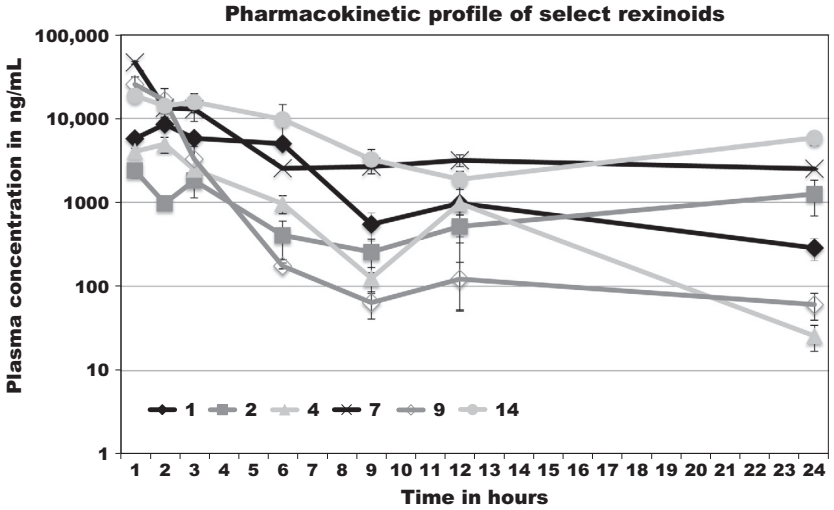

Figure 7. Plasma concentration of rexinoids over a 24 h time course after a single dose of 100 mg/kg.

Table 8. Solubilities and calculated pK_a for compounds analyzed in rats.

Compound	$\lambda_{max\ EtOH}$ (nm)	ε_{EtOH} ([mol/L]$^{-1}$·cm^{-1})	$\lambda_{max\ 10\%\ EtOH/Water}$ (nm)	$\varepsilon_{10\%\ EtOH/Water}$ ([mol/L]$^{-1}$·cm^{-1})	Water solubility at 20°C (μmol/L)	pK_a[1] Calc'd
1	260	17,000	260	14,000	0.28 ± 0.02	3.5
2	246	17,000	243	15,000	58 ± 1	−0.4
4	284	24,000	283	18,000	7.6 ± 0.1	3.9
7	252	20,000	243	19,000	49 ± 1	1.8
9	221 (sh)	19,000	220	25,000	67 ± 1	1.7
14	252	17,000	244	17,000	15 ± 1	1.1

A 2.0 mmol/L stock solution in ethanol of each compound was made from which ε was determined from a Beer's law plot of dilutions. A 10 μmol/L solution in 10% ethanol/water of each compound was also made by dissolving 0.020 mmol of each compound in 200 mL of ethanol and then diluting to 2 L with water. Dilutions of the 10 μmol/L solution in 10% ethanol/water were made to determine an equation for the Beer's law plot by linear regression. The water solubility of each compound was estimated by solving the linear regression equation from the Beer's law plot for the 10% ethanol/water solutions with the observed absorbance of saturated aqueous solutions of each compound. Water solubility estimates from measured absorbances are shown as the mean ± standard deviation or the last significant digit, whichever is greater.
[1]Calculated pK_a values, performed in Gaussian 9.0, using the thermodynamic cycle in Figure 1.

whereas the acrylic acid analog (**4**) possessed a water solubility (7.6 μmol/L) more similar to **1**. The two analogs possessing a pyrimidine ring, **7** and **9**, also possessed fairly high solubilities at 49 and 67 μmol/L, respectively. The mono-fluoro-unsaturated bexarotene analog (**14**) had an observed solubility of 15 μmol/L. While the analog solubilities were not proportional to C_{max} in all cases, and an analog's absorption and distribution may depend on several factors such as pK_a and lipophilicity, it is interesting to note that the analogs with two of the three highest measured water solubilities (**7** and **9**) possessed the two highest measured values for C_{max}.

We were also interested in assessing whether the pK_a of the analog could impact its absorption. Hence, we calculated each of the tested compound's pK_a values (Table 8 and Fig. 8). All analogs are weak acids, with the exception of **2** whose pK_a was fairly low at −0.4. It is generally known that the unionized form of compounds is more easily absorbed in the stomach. When disregarding **2**, the calculated pK_a values showed strong anticorrelation between C_{max}, AUC_{0-t}, and AUC_{0-inf}, with regression coefficients of −0.68, −0.79, and −0.72, respectively (Fig. 8). In addition, the compound possessing the lowest pK_a (**2**) also possessed the lowest measured C_{max}.

Expression comparison of compounds and vehicle demonstrate differential expression of genes after treatment of RXR ligands

Because the in vitro data hinted the analogs might have differential effects, and due to the fact that the PK profiles

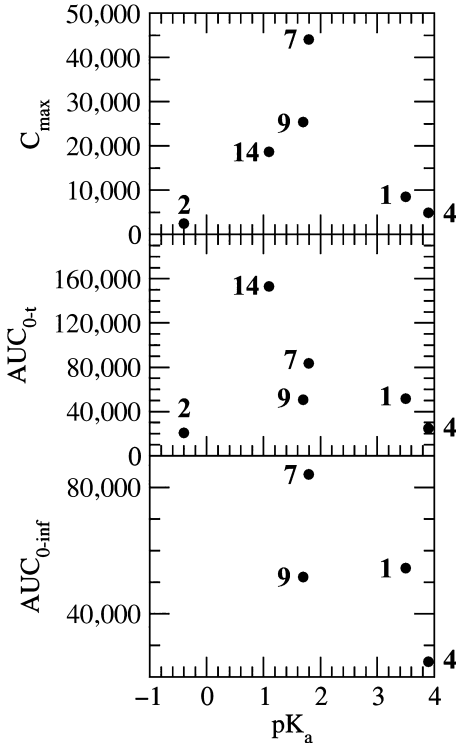

Figure 8. Plots of C_{max}, AUC_{0-t}, and AUC_{0-inf} versus calculated pK_a for **1**, **2**, **4**, **7**, **9**, and **14**. AUC, area under the curve.

and the chemical properties of the RXR ligands were so different, we further hypothesized that each analog could be inducing diverse cellular effects. In order to demonstrate that each analog was novel in its cellular and molecular effects, we analyzed the expression profiles induced in the rats after analog administration. The brains of the rats were snap frozen 24 h after the treatment and then RNA was extracted and subjected to sequencing analysis to compare expression between treatments. Our analysis demonstrated that each analog induced and repressed a different suite of genes (Fig. 9 and Table 9). For example, in Figure 9, rats treated with **7** demonstrated the most upregulation of genes (yellow and orange) compared to bexarotene-treated rats; and rats treated with **9** demonstrated the most disparate gene expression to rats treated with bexarotene. In Table 9, we see specific genes that are differentially regulated when rats are dosed with RXR ligands. For example, the gene *Stra6* is upregulated in the brains of rats treated with **9** and highly upregulated when treated with **2**, but slightly repressed in the brains of rats treated with bexarotene or **7**. Mir346, a small RNA implicated in inflammation, is downregulated in bexarotene-treated rats but upregulated in rats treated with **4**, **7**, and **9**. Table 9 outlines differential regulation of a wide variety of genes, demonstrating that these RXR ligands, although somewhat similar in structure, are varied in their induction of molecular events. Thus, these RXR ligands demonstrate differential effects at the molecular and cellular levels, as demonstrated by their expression profiles.

Discussion

We wished to explore not only the effects in vivo of analogs bearing a close resemblance to bexarotene–as with **2**, **7**, and **14**–but also analogs of other reported potent RXR agonists. While all three analogs of bexarotene, **2**, **7**, and **14**, possess electron withdrawing groups on the ring bearing the carboxylic acid, **7** relies on two nitrogen atoms of a pyrimidine ring, whereas both **2** and **14** possess fluorine atom(s) proximal to the carboxylic acid group. We examined not only the effects in vivo of the potent difluorinated **2** but we were also interested to see how effects might differ in comparison to **14** that places a single fluorine proximal to the carboxylic acid group of **1** and possesses one additional degree of unsaturation in the aliphatic ring of **1**. As for the other two chemical motifs from which we selected analogs to test in vivo, LGD100268 (**8**) differs from bexarotene by substituting a pyridine ring for the phenyl ring of bexarotene that bears the carboxylic acid group, and **8** also possesses a cyclopropyl ring bridging the two aromatic rings. In addition to a report showing **8** to be more potent than bexarotene in COS-1 cells by one order of magnitude (Boehm et al. 1995), there are numerous reports of **8** serving as an effective RXR agonist both in vitro (Boehm et al. 1995; Mu et al. 2000) and in vivo (Liu et al. 2002). In compound **9**, we devised an analog of **8** that possesses one additional nitrogen atom by substituting a pyrimidine ring for the pyridine ring of **8**. We were encouraged that cytotoxicity experiments (GreenScreen, Cyprotex, Watertown, MA) identified **9** to be the least toxic of all compounds evaluated prior to in vivo work, and we were eager to evaluate this compound's in vivo effects in comparison to **1**. Finally, we wished to assess a potent RXR agonist analog of CD3254 (**3**) that substituted a methyl group (**4**) for the hydroxyl group of **3** to determine if this type of biphenyl framework for a potent RXR agonist had similar or markedly different effects than **1**.

The analysis of the SREBP promoter transactivation data in cultured human cells, as compared with the rat in vivo lipid data, yields remarkable similarities. The most striking differences in the lipid profile in the rat model were seen in the triglyceride concentrations. For the rats treated with compound **4**, between 1 and 12 h results were similar to those treated with bexarotene. This is comparable to Figure 5, in which we can see that cells treated with compound **4** (with or without T0) show similar activation of the SREBP promoter when compared to

Table 9. Differential expression of genes in rat brain after 24 h treatment with RXR ligand.

Gene	Protein	1	2	4	7	9	14
Inmt	Indolethylamine *N*-methyltransferase	−0.23	1.93	−0.41	−0.82	−0.36	−0.13
Ccl6	Chemokine (C-C motif) ligand 6	0.054	0.66	−0.91	−1.46	−1.39	−1.68
Mta2	Metastasis-associated 1 family, member 2	0.97	1.88	−0.10	−1.36	−0.34	−1.45
Cyp26b1	Cytochrome P450 family 26, subfamily B, polypeptide 1	−0.020	1.94	0.15	−0.28	−0.07	−0.090
Stra6	Retinol-binding protein receptor	0.05	1.58	0.23	−0.05	0.13	0.22
Angpt14	Angiopoietin-related protein 4	0.18	0.28	−0.31	−1.11	−0.64	−1.43
Pdk4	mt pyruvate dehydrogenase lipoamide kinase isozyme 4	0.77	0.87	−0.04	−0.44	−0.07	−0.61
Nmb	Neuromedin B	0.166	1.28	0.33	−0.38	0.20	−1.00
Epha3	EPH receptor A3	−0.34	−0.89	−0.27	0.34	0.007	−0.49
Lyve1	Lymphatic vessel endothelial hyaluronan receptor 1	0.093	0.79	−0.13	−0.049	−0.097	−0.052
LOC689600	Uncharacterized and highly conserved	−0.52	−0.99	−0.43	0.53	−0.037	−0.55
Vom2r8	Vomeronasal 2 receptor, 8	−0.21	−0.27	−0.62	0.074	−0.85	−0.51
Mir346	microRNA 346	−0.12	0.002	0.81	0.17	0.52	0.30
Acot1	Acyl-CoA thioesterase 1	−0.31	−0.02	0.41	−0.93	−0.65	−1.14
Mir3556b	microRNA mir-3556b	−1.13	−0.95	−0.23	−0.38	−0.14	0.11
Cyp26a1	Cytochrome P450 26A1	0.46	1.00	0.061	−0.088	0.002	0.15
Abca1	ATP-binding cassette transporter ABCA1	−0.025	0.17	0.19	−2.06	−1.04	−1.78
Aurkb	Aurora kinase B	0.11	0.90	0.43	0.34	0.25	0.40
Ust5r	Integral membrane transport protein	−0.94	−1.68	−0.14	0.054	0.089	0.28
Upp1	Uridine phosphorylase 1	0.38	0.78	0.20	−0.700	0.055	−0.33
LOC500594	Ribosomal protein	−0.20	0.63	0.78	0.20	0.55	0.48
Rbp1	Retinol-binding protein 1	−0.48	0.62	−0.19	−0.58	−0.36	−0.63
Sycp2	Synaptonemal complex protein	−0.18	−0.25	0.24	0.048	0.69	−0.28
Alb	Albumin	−0.17	−2.90	−2.67	−0.46	−2.52	−2.54
Ifit3	Interferon-induced protein with tetratricopeptide repeats 3	−0.82	−0.88	0.50	−0.88	−0.083	−0.37
Arl11	ADP-ribosylation factor-like 11	0.072	−0.22	−0.017	−0.65	−0.13	−0.76
Scd1	Stearoyl-CoA desaturase-1	−0.54	−0.30	−0.007	−1.35	−1.20	−1.95
Mpeg1	Macrophage expressed gene 1	0.0023	−0.54	−0.94	0.44	0.17	−0.40
Lrrc4c	Leucine rich repeat containing	−0.19	−0.44	−0.50	0.71	0.11	−0.35
Sfrp5	Secreted frizzled-related protein 5	0.37	−0.27	−0.30	−0.20	0.51	0.60
Cav1	Caveolin	−0.39	0.18	0.62	0.75	−0.07	0.63
Emr4	Member of the EGF-TM7 family	0.14	−0.10	0.25	0.64	0.45	0.70
Dlx2	Distal-less homeobox 2	−0.052	0.92	1.18	0.39	0.62	0.48
Nmu	Neuromedin U	0.074	0.44	−0.062	−0.50	−0.41	−0.24
Cga	Choriogonadotropin alpha	2.91	2.91	3.20	2.71	4.22	2.22

RNA sequencing was used to probe expression differences in brains in rats after 24 h of a single dose of analog. Expression data were analyzed using a general linear model to generate differential expression profiles utilizing a likelihood ratio test of significance of all coefficients. RXR, retinoid X receptor.

bexarotene. For the rats treated with compound **7**, lipid profiles are statistically identical to the rats treated with bexarotene, and the same relationship is seen in the cells treated either with or without T0. Finally, and most strikingly, cells treated with compound **14**, either with or without T0 had the highest transcriptional response in human cell culture; in rats, the triglyceride concentrations at 24 h were incredibly high (1589 ± 820.9 mg/dL), similar to the cells treated with this compound.

There are differences between the TRE activation profiles of the analogs at the two different concentrations (Fig. 3A and B). In general, the cells treated with 1×10^{-7} mol/L rexinoid seem to generate slightly more active TRE-based transcription. We speculate that at the high dose of 5×10^{-7} mol/L the rexinoids may be depleting the limiting pool of TR coactivators, perhaps including SRC1, SRC2, SRC3 (Stashi et al. 2014), TRAP100, and TRAP220 (Ito and Roeder 2001). Since there is endogenous RXR in the cells, some of those RXRs become active RXR-RXR homodimers, which then interact with these coactivators and more RXR-RXR homodimers complexed with coactivators will be formed at the higher dose. That pool of RXR-RXR homodimers will not bind the TRE, but still could influence TRE activity because they titrate away the limiting pool of coactivators that are in the cell, and those same coactivators are needed for the TRE-driven transcription (by the RXR-TR still bound to the TRE). This is because our assay system

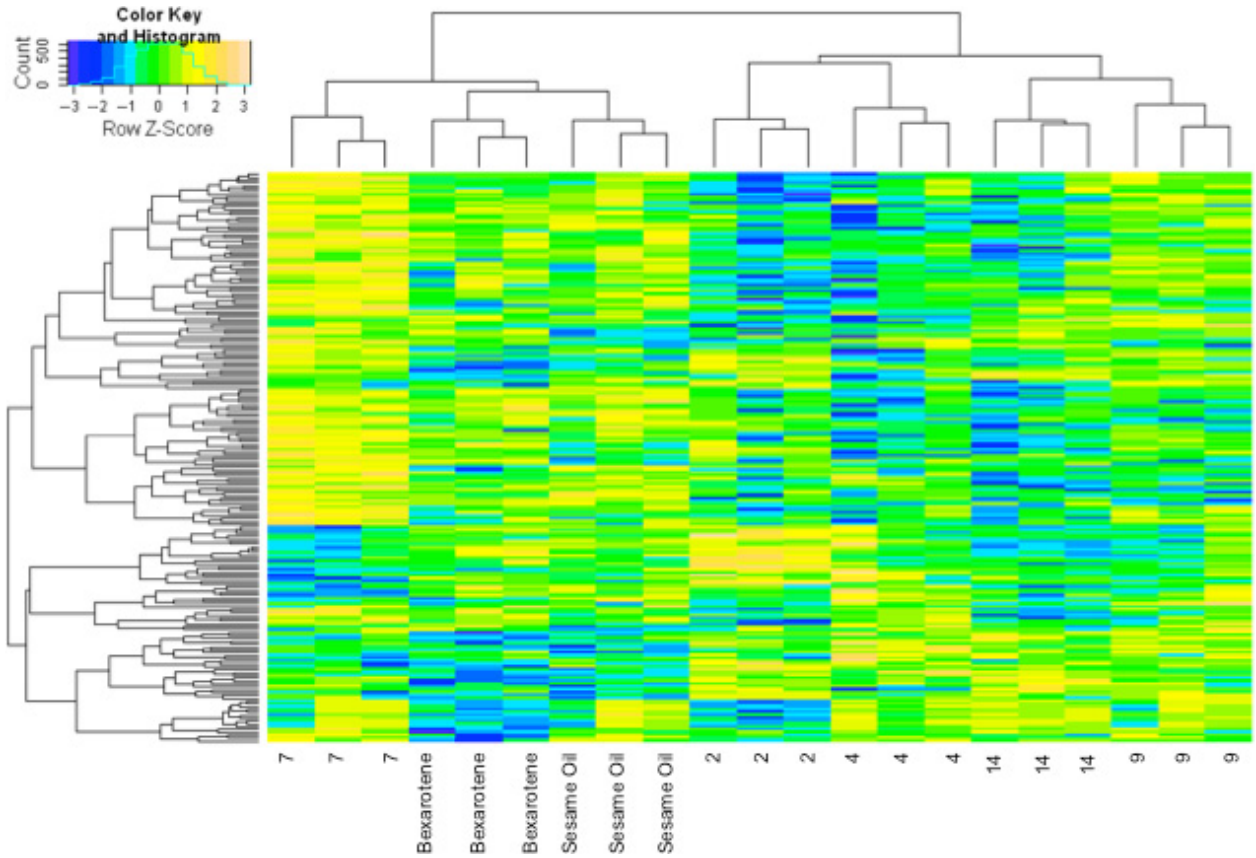

Figure 9. Differential expression analysis of rat brains after treatment with RXR agonists. RNA was isolated and expression determined using RNA sequencing from rat brains after 24 h of a one time treatment with vehicle or compound. A likelihood ratio test of significance of all coefficients demonstrated 200 genes that were detected to be differentially expressed at $P < 1.0 \times 10^{-3}$, fdr < 0.3 utilizing a general linear model of expression comparison. RXR, retinoid X receptor.

measures the active RXR-TR bound to the TRE that then stimulates transcription of the luciferase reporter gene, but the induction of luciferase is also influenced by the available pool of coactivators. In support of this hypothesis, we overexpressed the SRC-1 coactivator and observed that the repressive effects of high-dose rexinoid treatment were reversed (data not shown).

All of the analogs inhibit TSH synthesis to the same extent in our rat model (Fig. 7), as opposed to the analogs that inhibit TRE-mediated transcription differentially in cell culture. TSH is synthesized in the pituitary gland, and its promoter contains several regulatory regions, including a negative regulatory element, suppressed by T3 binding to TR as well as RXR repression, shown to be mediated by ligand (Haugen et al. 1997). This repression in the pituitary is intriguingly regulated by RXRγ (Haugen et al. 1997), indicating perhaps that each analog can bind RXRγ with similar affinity. In contrast, HCT-116 cells contain endogenous RXRα and to a lesser extent RXRβ (van der Leede et al. 1993) and lack RXRγ; Figure 4 hints that an RXRα/TR heterodimer is differentially inhibited by different rexinoids, which have EC_{50}s ranging from 13 to 109 nmol/L (Table 1) (Wagner et al. 2009; Furmick et al. 2012; Jurutka et al. 2013). Thus, we have demonstrated that RXR ligands with different structures can potentially mitigate some of the hypothyroid side effects, at least in T3-TRE-responsive tissues.

Conclusion

Because of the wide-ranging applications of bexarotene (**1**), not only in treating several human cancers but also impacting pathways implicated in neurological disorders, and the concomitant side effects of hypothyroidism and raised triglycerides, we undertook an in vitro and in vivo evaluation of five potent RXR-selective agonists (rexinoids) we reported recently (**2**, **4**, **7**, **9**, and **14**). Prior to in vivo experiments, we tested all compounds, and bexarotene (**1**), for toxicity and mutagenicity in the Cyprotex GreenScreen assay, whose results indicated that the com-

pounds were not expected to be more toxic than **1**. Indeed, this toxicity screen indicated that **9** was the least toxic of all compounds. We had also screened several of the novel rexinoids (Fig. 2) in cell-based TRE and SREBP assays whose results suggested that many of the novel rexinoids (Figs. 3–5) might show markedly different TSH and lipid profiles in vivo. A rigorous examination of the PK, TSH, cholesterol, HDL, LDL, and triglyceride profiles in Sprague–Dawley rats for the five potent rexinoids (**2**, **4**, **7**, **9**, and **14**) in comparison to bexarotene (**1**) demonstrates that while some features are similar among the rexinoids and **1**–such as the TSH profiles–other features, such as the PK and triglyceride profiles, are significantly different. In fact, compounds **4** and **9** had statistically lower triglyceride levels at 24 h than **1**, and **14** had a statistically much higher triglyceride level at 24 h than **1**. Additionally, we observed that compounds **7** and **9** had a significantly higher C_{max} than **1**, whereas compound **2** had a much lower C_{max} than **1**. This difference in PK profile compelled us to investigate factors that might explain the difference between these compounds. Thus, we examined the water solubility of the five rexinoids (**2**, **4**, **7**, **9**, and **14**) and **1** and we also modeled them to arrive at calculated pK_a values. The water solubility experiments showed that the pyrimidine-ring containing compounds (**7** and **9**) possessed two of the three highest measured water solubilities, which might reasonably contribute to their high observed C_{max} values. Furthermore, even though **2** possessed the second highest measured water solubility, the pK_a calculations suggested that **2** was the most acidic which might also reasonably contribute to its low observed C_{max} value, despite its relatively good solubility. Additionally, we extracted and sequenced RNA from the brains of rats treated with bexarotene, novel rexinoids (**2**, **4**, **7**, **9**, and **14**), and vehicle, and data from these experiments indicated significant differences in upregulation and repression of various genes between analogs. Of particular note, compound **7** displayed the greatest upregulation of genes across the table, and compound **9** showed the greatest difference in upregulation and repression of genes in comparison to bexarotene. Taken together, these results suggest that several of the five novel rexinoids–particularly, **4**, **7**, and **9**–possess PK and triglyceride profiles, as well as physical characteristics that in comparison to **1** make them compelling candidates for further preclinical studies.

Acknowledgements

This work was supported by the National Institutes of Health National Cancer Institute (Grant 1 R15 CA139364-01A2) and the Della L. Thome Memorial Foundation. Computer time was provided by USF Research Computing and XSEDE.

Disclosures

The authors declare the following competing financial interest(s): Patent applications covering **2**, **4**, **7**, **9**–**12**, and **14** have been applied for on behalf of the Arizona Board of Regents.

References

Boehm MF, Zhang L, Zhi L, McClurg MR, Berger E, Wagoner M, et al. (1995). Design and synthesis of potent retinoid X receptor selective ligands that induce apoptosis in leukemia cells. J Med Chem 38: 3146–3155.

Bolko K, Zvonar A, Gasperlin M (2014). Simulating the digestion of lipid-based drug delivery systems (LBDDS): overview of in vitro lipolysis models. Acta Chim Slov 61: 1–10.

Castillo AI, Sanchez-Martinez R, Moreno JL, Martinez-Iglesias OA, Palacios D, Aranda A (2004). A permissive retinoid X receptor/thyroid hormone receptor heterodimer allows stimulation of prolactin gene transcription by thyroid hormone and 9-*cis*-retinoic acid. Mol Cell Biol 24: 502–513.

Cramer PE, Cirrito JR, Wesson DW, Lee CY, Karlo JC, Zinn AE, et al. (2012). ApoE-directed therapeutics rapidly clear beta-amyloid and reverse deficits in AD mouse models. Science 335: 1503–1506.

Dragnev KH, Petty WJ, Shah SJ, Lewis LD, Black CC, Memoli V, et al. (2007). A proof-of-principle clinical trial of bexarotene in patients with non-small cell lung cancer. Clin Cancer Res 13: 1794–1800.

Eisai (2001) Targretin® (bexarotene) capsules, 75 mg insert. FDA Drug Insert Reference ID: 2946940.

Esteva FJ, Glaspy J, Baidas S, Laufman L, Hutchins L, Dickler M, et al. (2003). Multicenter phase II study of oral bexarotene for patients with metastatic breast cancer. J Clin Oncol 21: 999–1006.

Fan J, Donkin J, Wellington C (2009). Greasing the wheels of abeta clearance in alzheimer's disease: the role of lipids and apolipoprotein E. BioFactors 35: 239–248.

Fantini J, Di Scala C, Yahi N, Troadec JD, Sadelli K, Chahinian H, et al. (2014). Bexarotene blocks calcium-permeable ion channels formed by neurotoxic alzheimer's ss-amyloid peptides. ACS Chem Neurosci 5: 216–224.

Fitz NF, Cronican AA, Lefterov I, Koldamova R (2013). Comment on "ApoE-directed therapeutics rapidly clear beta-amyloid and reverse deficits in AD mouse models". Science 340:924-c.

Forman BM, Yang CR, Au M, Casanova J, Ghysdael J, Samuels HH (1989). A domain containing leucine-zipper-like motifs mediate novel in vivo interactions between the thyroid hormone and retinoic acid receptors. Mol Endocrinol 3: 1610–1626.

Forman BM, Umesono K, Chen J, Evans RM (1995). Unique response pathways are established by allosteric interactions among nuclear hormone receptors. Cell 81: 541–550.

Frisch MJ, Trucks GW, Schlegel HB, Scuseria GE, Robb MA, Cheeseman JR, et al. (2009). Gaussian 09. revision D.01. Gaussian, Inc., Wallingford CT.

Furmick JK, Kaneko I, Walsh AN, Yang J, Bhogal JS, Gray GM, et al. (2012). Modeling, synthesis and biological evaluation of potential retinoid X receptor-selective agonists: novel halogenated analogues of 4-[1-(3,5,5,8,8-pentamethyl-5, 6,7,8-tetrahydro-2-naphthyl)ethynyl]benzoic acid (bexarotene). ChemMedChem 7: 1551–1566.

Goodman AB (1994). Retinoid dysregulation as a cause of schizophrenia. Am J Psychiatry 151: 452–453.

Haugen BR, Brown NS, Wood WM, Gordon DF, Ridgway EC (1997). The thyrotrope-restricted isoform of the retinoid-X receptor-gamma1 mediates 9-*cis*-retinoic acid suppression of thyrotropin-beta promoter activity. Mol Endocrinol 11: 481–489.

Heneka MT, Sastre M, Dumitrescu-Ozimek L, Hanke A, Dewachter I, Kuiperi C, et al. (2005). Acute treatment with the PPARgamma agonist pioglitazone and ibuprofen reduces glial inflammation and Abeta1-42 levels in APPV717I transgenic mice. Brain 128: 1442–1453.

Holtzman DM (2004). In vivo effects of ApoE and clusterin on amyloid-beta metabolism and neuropathology. J Mol Neurosci 23: 247–254.

Howell SR, Shirley MA, Grese TA, Neel DA, Wells KE, Ulm EH (2001). Bexarotene metabolism in rat, dog, and human, synthesis of oxidative metabolites, and in vitro activity at retinoid receptors. Drug Metab Dispos 29: 990–998.

Ito M, Roeder RG (2001). The TRAP/SMCC/mediator complex and thyroid hormone receptor function. Trends Endocrinol Metab 12: 127–134.

Johnson LM, Bankaitis VA, Emr SD (1987). Distinct sequence determinants direct intracellular sorting and modification of a yeast vacuolar protein. Cell 48: 875–885.

Jurutka PW, Kaneko I, Yang J, Bhogal JS, Swierski JC, Tabacaru CR, et al. (2013). Modeling, synthesis, and biological evaluation of potential retinoid X receptor (RXR) selective agonists: novel analogues of 4-[1-(3,5,5,8,8-pentamethyl-5, 6,7,8-tetrahydro-2-naphthyl)ethynyl]benzoic acid (bexarotene) and (E)-3-(3-(1,2,3,4-tetrahydro-1,1,4,4,6-pentamethylnaphthalen-7-yl)-4-hydroxypheny l)acrylic acid (CD3254). J Med Chem 56: 8432–8454.

Koldamova R, Staufenbiel M, Lefterov I (2005). Lack of ABCA1 considerably decreases brain ApoE level and increases amyloid deposition in APP23 mice. J Biol Chem 280: 43224–43235.

Lala DS, Mukherjee R, Schulman IG, Koch SS, Dardashti LJ, Nadzan AM, et al. (1996). Activation of specific RXR heterodimers by an antagonist of RXR homodimers. Nature 383: 450–453.

van der Leede B-JM, van den Brink CE, Van der Saag PT (1993). Retinoic acid receptor and retinoid X receptor expression in retinoic acid-resistant human tumor cell lines. Mol Carcinogen 2: 112–122.

Lehmann JM, Zhang XK, Graupner G, Lee MO, Hermann T, Hoffmann B, et al. (1993). Formation of retinoid X receptor homodimers leads to repression of T3 response: hormonal cross talk by ligand-induced squelching. Mol Cell Biol 13: 7698–7707.

Leid M, Kastner P, Chambon P (1992). Multiplicity generates diversity in the retinoic acid signalling pathways. Trends Biochem Sci 17: 427–433.

Lemon BD, Freedman LP (1996). Selective effects of ligands on vitamin D3 receptor- and retinoid X receptor-mediated gene activation in vivo. Mol Cell Biol 16: 1006–1016.

Lerner V, Miodownik C, Gibel A, Kovalyonok E, Shleifer T, Goodman AB, et al. (2008). Bexarotene as add-on to antipsychotic treatment in schizophrenia patients: a pilot open-label trial. Clin Neuropharmacol 31: 25–33.

Liu S, Ogilvie KM, Klausing K, Lawson MA, Jolley D, Li D, et al. (2002). Mechanism of selective retinoid X receptor agonist-induced hypothyroidism in the rat. Endocrinology 143: 2880–2885.

MacDonald PN, Dowd DR, Nakajima S, Galligan MA, Reeder MC, Haussler CA, et al. (1993). Retinoid X receptors stimulate and 9-*cis* retinoic acid inhibits 1,25-dihydroxyvitamin D3-activated expression of the rat osteocalcin gene. Mol Cell Biol 13: 5907–5917.

Mangelsdorf DJ, Evans RM (1995). The RXR heterodimers and orphan receptors. Cell 83: 841–850.

Mangelsdorf DJ, Umesono K, Evans RM (1994). The retinoid receptors. Pp. 319–349 *in* MB Sporn, AB Roberts and DS Goodman, eds. The retinoids: biology, chemistry, and medicine. Academic Press, New York, NY.

Marenich AV, Cramer CJ, Truhlar DG (2009). Universal solvation model based on solute electron density and on a continuum model of the solvent defined by the bulk dielectric constant and atomic surface tensions. J Phys Chem B 113: 6378–6396.

McFarland K, Spalding TA, Hubbard D, Ma JN, Olsson R, Burstein ES (2013). Low dose bexarotene treatment rescues

dopamine neurons and restores behavioral function in models of Parkinson's disease. ACS Chem Neurosci 4: 1430–1438.

Merrick JP, Moran D, Radom L (2007). An evaluation of harmonic vibrational frequency scale factors. J Phys Chem A 111: 11683–11700.

Mu YM, Yanase T, Nishi Y, Hirase N, Goto K, Takayanagi R, et al. (2000). A nuclear receptor system constituted by RAR and RXR induces aromatase activity in MCF-7 human breast cancer cells. Mol Cell Endocrinol 166: 137–145.

Nahoum V, Perez E, Germain P, Rodriguez-Barrios F, Manzo F, Kammerer S, et al. (2007). Modulators of the structural dynamics of the retinoid X receptor to reveal receptor function. Proc Natl Acad Sci USA 104: 17323–17328.

Price AR, Xu G, Siemienski ZB, Smithson LA, Borchelt DR, Golde TE, et al. (2013) Comment on "ApoE-directed therapeutics rapidly clear beta-amyloid and reverse deficits in AD mouse models". Science 340:924-d.

Remenyi A, Scholer HR, Wilmanns M (2004). Combinatorial control of gene expression. Nat Struct Mol Biol 11: 812–815.

Repa JJ, Liang G, Ou J, Bashmakov Y, Lobaccaro JM, Shimomura I, et al. (2000). Regulation of mouse sterol regulatory element-binding protein-1c gene (SREBP-1c) by oxysterol receptors, LXRalpha and LXRbeta. Genes Dev 14: 2819–2830.

Sánchez-Juan C, Gamón ER, Fabra XG, de Miquel VA, Galera RA, García J-F (2007). Central hypothyrodism and dyslipidemia induced by bexarotene in patients with cutaneous T-cell lymphoma. Endocrin Abst 14: P476.

Trapnell C, Roberts A, Loyal Goff L, Pertea G, Kim D, Kelley DR, Pimentel H, Salzberg SL, Rinn JL, Pachter L (2012). Differential gene and transcript expression analysis of RNA-seq experiments with TopHat and Cufflinks. Nature Protocols 7: 562–578.

Sherman SI, Gopal J, Haugen BR, Chiu AC, Whaley K, Nowlakha P, et al. (1999). Central hypothyroidism associated with retinoid X receptor-selective ligands. N Engl J Med 340: 1075–1079.

Shields GC, Seybold P, eds (2013). Computational approaches for the prediction of pKa values. CRC Press, Boca Raton, FL.

Stashi E, York B, O'Malley BW (2014). Steroid receptor coactivators: servants and masters for control of systems metabolism. Trends Endocrinol Metab 25:337–347.

Svensson S, Ostberg T, Jacobsson M, Norstrom C, Stefansson K, Hallen D, et al. (2003). Crystal structure of the heterodimeric complex of LXRalpha and RXRbeta ligand-binding domains in a fully agonistic conformation. EMBO J 22: 4625–4633.

Tai LM, Koster KP, Luo J, Lee SH, Wang YT, Collins NC, et al. (2014). Amyloid-beta pathology and APOE genotype modulate retinoid X receptor agonist activity in vivo. J Biol Chem 289: 30538–55.

Talayero BG, Sacks FM (2011). The role of triglycerides in atherosclerosis. Curr Cardiol Rep 13: 544–552.

Tesseur I, Lo AC, Roberfroid A, Dietvorst S, Van Broeck B, Borgers M, et al. (2013). Comment on "ApoE-directed therapeutics rapidly clear beta-amyloid and reverse zdeficits in AD mouse models". Science 340: 924-e.

Thompson PD, Jurutka PW, Haussler CA, Whitfield GK, Haussler MR (1998). Heterodimeric DNA binding by the vitamin D receptor and retinoid X receptors is enhanced by 1,25-dihydroxyvitamin D3 and inhibited by 9-*cis*-retinoic acid. Evidence for allosteric receptor interactions. J Biol Chem 273: 8483–8491.

Thompson PD, Remus LS, Hsieh JC, Jurutka PW, Whitfield GK, Galligan MA, et al. (2001). Distinct retinoid X receptor activation function-2 residues mediate transactivation in homodimeric and vitamin D receptor heterodimeric contexts. J Mol Endocrinol 27: 211–227.

Trapnell C, Roberts A, Loyal Goff L, Pertea G, Kim D, Kelley DR, Pimentel H, Salzberg SL, Rinn JL, Pachter L (2012). Differential gene and transcript expression analysis of RNA-seq experiments with TopHat and Cufflinks. Nature Protocols 7: 562–578.

Tsika RW, Bahl JJ, Leinwand LA, Morkin E (1990). Thyroid hormone regulates expression of a transfected human alpha-myosin heavy-chain fusion gene in fetal rat heart cells. Proc Natl Acad Sci USA 87: 379–383.

Veeraraghavalu K, Zhang C, Miller S, Hefendehl JK, Rajapaksha TW, Ulrich J, et al. (2013). Comment on "ApoE-directed therapeutics rapidly clear beta-amyloid and reverse deficits in AD mouse models". Science 340: 924f.

de Vries-van der Weij J, deHaan W, Hu L, Kuif M, Oei HL, van der Hoorn JW, et al. (2009). Bexarotene induces dyslipidemia by increased very low-density lipoprotein production and cholesteryl ester transfer protein-mediated reduction of high-density lipoprotein. Endocrinology 150:2368–2375.

Wagner CE, Jurutka PW, Marshall PA, Groy TL, van der Vaart A, Ziller JW, et al. (2009). Modeling, synthesis and biological evaluation of potential retinoid X receptor (RXR) selective agonists: novel analogues of 4-[1-(3,5,5,8,8-pentamethyl-5,6,7,8-tetrahydro-2-naphthyl)ethynyl]benzoic acid (bexarotene). J Med Chem 52: 5950–5966.